

STC-IDS: Spatial-Temporal Correlation Feature Analyzing based Intrusion Detection System for Intelligent Connected Vehicles

Mu Han*, *Member, IEEE*, Pengzhou Cheng, and Fengwei Zhang

Abstract—Intrusion detection is an important defensive measure for the security of automotive communications. Accurate frame detection models assist vehicles to avoid malicious attacks. Uncertainty and diversity regarding attack methods make this task challenging. However, the existing works have the limitation of only considering local features or the weak feature mapping of multi-features. To address these limitations, we present a novel model for automotive intrusion detection by spatial-temporal correlation features of in-vehicle communication traffic (STC-IDS). Specifically, the proposed model exploits an encoding-detection architecture. In the encoder part, spatial and temporal relations are encoded simultaneously. To strengthen the relationship between features, the attention-based convolution network still captures spatial and channel features to increase the receptive field, while attention-LSTM build important relationships from previous time series or crucial bytes. The encoded information is then passed to detector for generating forceful spatial-temporal attention features and enabling anomaly classification. In particular, single-frame and multi-frame models are constructed to present different advantages respectively. Under automatic hyper-parameter selection based on Bayesian optimization, the model is trained to attain the best performance. Extensive empirical studies based on a real-world vehicle attack dataset demonstrate that STC-IDS has outperformed baseline methods and cables fewer false-positive rates while maintaining efficiency.

Index Terms—In-vehicle networks (IVNs), Control area network (CAN), Intrusion detection system (IDS), Spatial-temporal features, Attention mechanism

I. INTRODUCTION

NOWADAYS, a large number of electronic control units (ECUs) have replaced the mechanical control units to manage the assorted functions of in-vehicle control systems. The ECUs are interconnected to exchange varied vehicle information with each other via networks referred to as in-vehicle networks (IVNs) such as controller area networks (CAN) [1]. Along with local interconnected network LIN

This research was supported by the following funds: Natural Science Fund for Colleges and Universities in Jiangsu Province [12KJD580002]; the Jiangsu Graduate Innovation Fund [KYLX1057]; the Key Research and Development Plan of Jiangsu Province in 2017 (Industry Foresight and Generic Key Technology) [BE2017035]. (Corresponding author: Mu Han.)

Mu Han is with the School of Computer Science and Communication Engineering and Jiangsu Key Laboratory of Security Technology for Industrial Cyberspace Jiangsu University, Zhenjiang 212013, China (e-mail: hanmu@ujs.edu.cn).

Pengzhou Cheng is with the School of Computer Science and Communication Engineering, Jiangsu University, Zhenjiang 212013, China (e-mail: pengzhouchengai@gmail.com).

Fengwei Zhang is with the Department of Computer Science and Engineering, Southern University of Science and Technology, Shenzhen 518000, China (e-mail: zhangfw@sustech.edu.cn).

and FlexRay, CAN is well-known and most employed as the de-factor standard for IVNs. [2]. It is noteworthy that CAN was developed as a broadcast-based communication protocol that supports the maximum baud rate up to 1Mb per-second. Furthermore, the fault-tolerant detection mechanism guarantees the stability of message transmission.

However, the CAN bus utilized in the automotive has the potential danger of being attacked, owing to security mechanisms such as encryption, access control, and authentication are not considered [3]. Cyber security is becoming a major concern for IVNs systems as increasingly more security researchers demonstrate their ability to launch attacks on actual vehicles. What can be investigated is many known attacks, even some unknown attacks, have been threatening various significant components of IVNs [3], [4], [5]. For instance, 360 cyber-attack Lab adopted electronic radio-frequency technology to successfully hack into Tesla in 2015 [6]. Miller *et al.* invaded the Jeep Cherokee's IVNs system using an open Wi-Fi port and reprogrammed the firmware of the ECU. They succeeded in taking control of a wide range of vehicle functions (e.g., disabling the brakes and stopping the engine), triggering a recall of 1.4 million vehicles [3]. Thereafter, the electric features lift, warning lights, airbag [7], and tire pressure monitoring system (TPMS) [8] have also become the target of attack. Incredibly, these attacks have multiple ways of being performed. As such, the study on the security of IVNs is attracting significant attention from security researchers.

Available methods are attempted to protect IVNs secure, of which, IDS as an effective defense method has attracted more attention from researchers [9]. Currently, a host of IDS schemes are rule-based, statistical. Although accuracy and efficiency are excellent about some common attacks, the passive characteristic and the constant need for updates result in a certain restriction [10]. With the increase in vehicle computing power and the maturity in machine learning (ML) technology, they promote the further development of IDS. Real-time, higher detection, and lower false-positive rates have been a fervent problem of research for deep learning-based in-vehicle IDS. Simultaneously, inadequate feature extraction and its complex network structure and more parameters, also are pending breakthroughs [11]. To address such issues, variants of IDS based on deep learning have been proposed in recent years [11], [12], [13]. However, these variants of IDS merely consider the partial features, either time-series of CAN ID or CAN data field. Moreover, spatial-temporal correlation features have been shown to better capture the details of the message in

anomaly detection [14], [15], [16], whereas how to create represent the relationship between spatial-temporal features becomes a vital concern to elevate detection performance in the automotive intrusion.

Thus, the purpose of this paper is to provide an enhanced anomaly detection model based on the spatial-temporal correlation features of CAN packets. Based on an encoding-detection architecture, the intuition first trained a boosted convolution LSTM parallel feature extraction model. Improved attention-based LSTM network (A-LSTM) captures the temporal features and builds important relationships from previous sequences or crucial bytes. Meanwhile, a reduced VGGNet network to learn the spatial features from CAN frames. Moreover, the attention convolution block (A-Conv2D) enables attaining a broad perspective through multi-channel features to refine feature mapping and then concentrate more on changes in crucial areas and ignore bytes that are regular and unchanging. Afterward, spatial-temporal correlations between features are established to feed into the detector as a two-class classification problem. Note that both single-frame and multi-frame models are considered in this paper to present different advantages respectively.

This paper makes the following contributions.

- 1) Based on analyzing spatial-temporal correlation features of CAN messages in detail, we propose an enhanced convolution LSTM spatial-temporal feature encoder with attention. The single-frame model automatically captures the important byte relationships of each CAN frame and uses convolution components to find where key bytes are. Moreover, the multi-frame model captures significant relationships from previous time series, in which the attention convolution block, assisted by spatial attention and channel attention, is able to snap changes in crucial areas.
- 2) Further, the detector achieves anomaly detection for the constructed representative spatial-temporal correlation features after multi-view learning. We evaluated the detection performance of our scheme using a publicly available real vehicle CAN dataset. We also compare it with the baseline model and show a significant improvement in detection performance and a reduction in false-positive rates and error rates.
- 3) By performing the injection attack in the same way, we calculated the detection efficiency of the model on real vehicles. The multi-frame model has sufficient ability to satisfy real-time detection. In addition, the single-frame model combined with database retrieval has the ability to trace anomalous ECUs.

The rest of this paper is organized as follows. Section II presents a discussion of related work on CAN-based IDS. Section III introduces the CAN bus protocol, vulnerability, and analyzes the CAN frame with spatial-temporal. Section IV proposes the parallel network model based on spatial-temporal features analysis. The experiment result of the proposed model on the public real-vehicle dataset is described in Section V. Finally, we conclude this study and look ahead at in-vehicle IDS potential perspectives.

II. RELATED WORK

In this section, we provide an in-depth discussion about the research situation in anomaly detection and intrusion detection for in-vehicle CAN communication systems. They are divided into four categories, namely specification-based, fingerprint-based, statistical-based and machine learning-based approaches, as summarized in Table I.

A. Intrusion Detection Model based on Specification

The specification-based IDS focuses on defining system specifications, such as protocols and frame formats. When packets mismatch the system specification, an exception alarm is raised. In 2016, Dagan *et al.* [18] introduced an anti-spoofing system that detects malicious messages using each ECU, i.e., by detecting CAN message ID that was not sent by the ECU itself. Thereafter, the ECU informs the IDS and an interrupt pulse is sent to the CAN bus to overwrite the spoofed message. However, each ECU undertakes the IDS role, which increases a certain burden on communication.

In 2018, Studnia *et al.* [17] presented a signature-based IDS which utilize a list of signature derived from CAN dataset. However, this method is subject to the limitation that the length of the CAN bus word may not be known a priori. Recently, Olufowobi *et al.* [13] proposed a real-time IDS based on specification. The algorithm no longer depends on predefined specifications to detect anomalies, while observing CAN traffic to extract the timing model, yet exhibits relatively poor performance in real attack dataset.

B. Intrusion Detection Model based on Fingerprint

The fingerprint-based approaches are mainly based on profiles defined by ECU characteristics to implement anomaly detection. In 2016, Cho and Shin [19] proposed clock-based IDS to analyze ECUs periodic frequency. The method established the ECUs clock baseline through the recursive least squares algorithm (RLS) to detect intrusion. But it workable only to periodic messages excluding non-periodic messages.

Interestingly, Cho *et al.* [20] found a method to use the physical layer data of CAN communication to establish the electrical signal characteristics of each ECU, and harness these signal characteristics as the fingerprint of the ECU to in 2018. Regrettably, as the vehicle ages, the electrical characteristics may change and therefore the IDS needs to keep updating.

C. Intrusion Detection Model based on Statistical

Unlike upon methods, the statistics-based approach implements anomaly detection by means of statistical information obtained from CAN traffic at the network level. Song *et al.* [21] introduced a lightweight IDS in 2016 that detected anomalies by monitoring the abnormally shortened intervals between messages. Although the proposed algorithm could have highly sensitive to common injection attacks and low computing cost, it cannot detect irregular incoming messages.

Furthermore, Young *et al.* [22] comprehensively analyzed the frequency characteristics of CAN messages in various driving modes, such as reverse, acceleration and hold speed, and

TABLE I: COMPARISON OF IN-VEHICLE INTRUSION DETECTION SYSTEMS

Categories	Research work	Technique	Evaluation Data	Contribution	Limitation
Specification based	Studnia <i>et al.</i> [17]	a list of signatures derived from CAN data set	real	automatically generating a set of forbidden sequences	the length of CAN bus words may not be known a priori
	Dagan <i>et al.</i> [18]	An anti-spoofing system detects CAN message IDs by each ECU that are not sent by the ECU itself	real and simulation	Effective resistance to spoofing attacks	Each ECU takes on the IDS role, adding a certain burden to communication
	Olufowobi <i>et al.</i> [13]	worst-case response time analysis	real and synthesized	real-time parameter estimation algorithm developed in a black-box approach	high false positive rate and relatively low performance on open dataset
Fingerprint based	Cho and Shin [19]	analyzed the clock skew of ECUs	real and simulation	proposed an ECU pro-filing method according to electrical signal characteristics	workable only to periodic messages excluding non-periodic messages
	Choi <i>et al.</i> [20]	established the electrical signal features of each ECU based on time domain and frequency domain	real and simulation	effective of making a distinction between ECU malfunctions and a bus-off attack	The electrical properties of the vehicle may change as it ages, necessitating correction.
Statistics based	Song <i>et al.</i> [21]	analyzed the time-intervals of the CAN messages	real and synthesized	offered effectiveness of the method for injection attack detection	workable only to periodic messages excluding non-periodic messages
	Young <i>et al.</i> [22]	analyzed the time-intervals in the frequency domain	real	Improved frequency-based injection attack detection method	high false positive rate, and only identify injection attack
ML & DL based	Kang <i>et al.</i> [23]	deep belief network (DBN)	simulation	Presented unsupervised statistical feature extraction algorithms for ECU messages	Extremely time-consuming in the training phase, evaluation only based on simulation data
	Yang <i>et al.</i> [24]	Signature-based and anomaly-based Multilayer Hybrid IDS	real	Proposed an IDS that is effective for attacks on both in-vehicle and external networks	spatial-temporal features and important regional features are ignored
	Tariq <i>et al.</i> [25]	convolutional LSTM Network and transfer learning	real	Improved performance of unknown attack detection	Known attacks have poor relative detection performance
	Pawelec <i>et al.</i> [26]	LSTM prediction at the bit level	real	avoided reverse engineering proprietary encodings	Limited attack detection range
	Qin <i>et al.</i> [12]	LSTM network and five loss function	real	Presented two predicted model on different data format	relatively poor detection accuracy
	Song <i>et al.</i> [11]	deep CNN	real	Reduced Inception-resent model complexity to adapt IDS and improve detection performance	The spatial-temporal relationship of CAN frames is ignored
	STC-IDS (Ours)	parallel convolutional LSTM attention network	real	Important concerns for spatial-temporal features and crucial features	more unknown attacks are ignored

then proposed a frequency-based intrusion detection system. In spite of the high detection accuracy, there is a high false alarm rate. Manifestly, an IDS based on conditional statistical relationship analysis to learn the normal behavior of the system can detect manipulations and incorrect payload values [27], but still does not satisfy the high detection rate and low latency required by present-day IVNs for anomalous traffic.

D. Intrusion Detection Model based on Deep Learning

Machine learning (ML) and Deep learning (DL) based intrusion detection systems are an excellent option for extracting and learning normal and abnormal behavior, and then providing models to detect and predict attacks. Kang *et al.* [23] preprocessed normal and simulated attack data and construct a deep confidence network under unsupervised learning to detect if anomalies deviate from normal. Relatively however, inefficient and only validation of simulation data is not sufficient.

In 2019, Pawelec *et al.* [26] proposed a 3-layer LSTM neural network to predict the data payload for each CAN ID, which avoided reverse engineering proprietary encoding. Similarly, Qin *et al.* [12] also implemented anomaly detection for CAN bus based on timing features by LSTM and re-considered two data formats of CAN frames. Like Pawelec's method, both are implemented at the CAN bits level, but they both consider only timing characteristics and have relatively poor

detection performance. Recently, convolution neural network (CNN) have been implemented to traffic detection and praised for their high detection efficiency [28].

Song *et al.* [11] presented a reduced inception resent to construct an IDS capable of detecting spoofing and denial of service (DoS) attacks in a continuous pattern of vehicular traffic. Since the assistance of spatial-temporal relation is not taken into account, there is still room for improvement in the false positive rate. In other studies, Tariq *et al.* [25] introduced a convolution LSTM-based intrusion detection method. Although it displayed excellent detection performance in unknown attack than transfer learning, known attacks performance relatively worse that may be caused by the relevance of the CAN message features being discarded. Moreover, a multi-tiered hybrid IDS that incorporates a signature-based IDS and an anomaly-based IDS is proposed to detect both known and unknown attacks on vehicular networks by Yang *et al.* [24] in 2021. Their model has been proven that is effective for attacks on both in-vehicle and external networks. However, modeling with spatial-temporal features might take performance a step further.

However, The ML&DL methods mentioned above differ in the mode of selecting the detection domain of a message, typically the detection arbitration domain proposed by Song *et al.* [11], the detection data domain proposed by Qin *et al.* [12], and the spatial-temporal feature extraction proposed

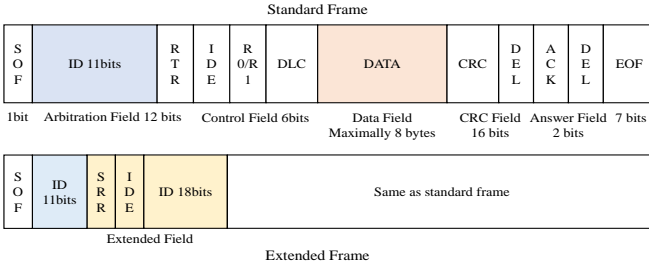


Fig. 1: Two forms of CAN data frame, standard frame and extended frame.

by Tariq *et al.* [25], which is similar to our work. In a nutshell, traditional methods based on specification, fingerprint, and statistical, have limitations in terms of reliance on anomaly feature libraries, message frequency, message time domain, and fingerprint information. Instead, it is imperative in the ML&DL area to improve automotive IDS detection performance and reduce false positives by complementing spatial-temporal features in a limited message communication mode. Furthermore, the model trained with limited spatial-temporal features will not effectively improve the detection performance.

Considering the nature of attention mechanisms to capture essential features, the generation of spatial-temporal attention features is one of the potential ways to address the above problem [12]. However, modeling the normal behavior of CAN packets in combination with spatial-temporal attention features and then discovering the difference between anomalies and target traffic is still one of the ways to improve in-vehicle IDS.

III. AN IN-DEPTH OVERVIEW OF CAN BUS DATASET

A. Vulnerabilities of In-Vehicle Networks

Intelligent Connected Vehicles (ICV), integrating modern computing and communication technologies, is designed to improve user experience and driving safety. As the most significant communication medium, the CAN is the most prevalent bus topology network employed in contemporary vehicles owing to its low cost and complexity, high reliability, and fault-tolerance characteristics [29]. All ECUs, connected to the CAN bus, are capable of exchanging messages in the form of data frames [30]. Fig. 1 presents the structure of a CAN message, consisting of seven fields [31]: 1) start of frame (1 bit); 2) arbitration field (12 bits for standard frames, 29 bits for extended frames); 3) control field (6 bits); 4) data field (Maximally 8 bytes); 5) cyclic redundancy code (CRC) field; 6) acknowledge (ACK) field; and 7) end of frame.

In the entire CAN frame, the most important is the arbitration field and the data field, as the arbitration field determines the priority of the message [32], shown in Fig. 2(a); the data field contains the actual transmitted data that defines the node actions. Moreover, if an error is detected by CRC field, the receiving node will discard the received error message, while the sending node will only assume a transient fault on the bus and enter arbitration to resend the message frame [33], [34], shown in Fig. 2(b). To guarantee the system consistency,

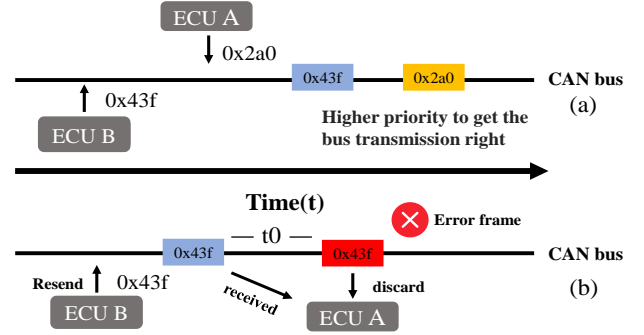


Fig. 2: Conceptual diagram of the message priority and CRC detection.

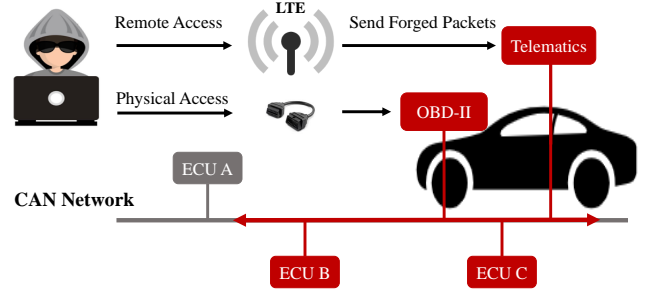


Fig. 3: The scenario in which an attacker performs an injection attack can be a remote attack or a physical attack can be implemented.

the ECU broadcasts messages at regular intervals in spite of the data values have not changed. However, security problems were poor-needly thought out at the beginning of the CAN bus design [35], including its broadcast transmission strategy, lack of authentication and encryption, and unsecured priority scheme. Hence, many network traffic injection attacks are possible.

This directly motivates the adversary to attack in-vehicle networks in a variety of ways, as shown in Fig.3 that not only through the OBD-II port for physical attacks but also implement a remote attack easily (e.g., Wi-Fi or Bluetooth). Types of such attacks include flooding the bus with messages designed to circumvent legitimate messages or using spoofed bus identifiers with invalid information. Furthermore, there are more sophisticated and stealthy attacks. These attacks appear to be legitimate traffic sequences that are tough to distinguish from normal traffic.

Once the attacker has successfully compromised, it has the opportunity to forge ECU nodes and take control of incumbent nodes to inject nefarious messages. In the CAN protocol, the connected nodes are synchronized with the current vehicle state by accepting the data field bits of the frame [11]. Consequently, in order to successfully deceive the ECU, the adversary must insert tampering messages in a high frequency and priority manner by following the target CAN ID message immediately after the message. If the attacker injects a high-priority CAN frame, of which the data field is populated with a status command to turn off the “wiper”, the driver loses

TABLE II: OVERVIEW OF CAR-HACKING dataset

Attack type	Normal messages	Injected messages
Dos attack	3078250	587521
Fuzzy attack	3347013	491847
RPM attack	2766522	597252
Gear attack	2290185	654897

TABLE III: PARTIAL ECU TRANSMISSION, RECEPTION AND TIME CYCLE OF AN AUTOMOTIVE BRAND

ID	Transmitter	periods	Receiver
0x101	EMS	10	TCU, ESP, EPB, T-BOX
0x278	EMS	10	TCU, GSM, ABS, ESP, EPS, EPB, PEPS
0x281	EMS	100	TCU, AC, ICU, HUD, T-BOX
0x1A0	TCU	10	EMS, GSM, ESP, EPB, PEPS, DRC, PDC
0x211	ESP	10	TCU, ESP, EPB, T-BOX
...
0x2EA	ABS	20	EMS, TCU, EPB, ICU, T-BOX, APA
0x68A	NVS	500	HUD, PSW

judgment in rainy conditions while driving at high speed, which would be a life-threatening attack.

B. Spatial-Temporal Correlation Feature Analyzing for CAN dataset

In this paper, we utilized car-hacking dataset which is published by Song *et al.* [36]. This dataset is injected with four attacks, respectively DoS attack, Fuzzy attack, spoofing attack including RPM and GEAR, as illustrated in Fig.4. The detailed injection rules are as follows.

- 1) DoS attack: The DoS attack in the dataset is to inject a high priority message with a '0x000' CAN ID every 0.3 milliseconds, with the data field populated with 0.
- 2) Fuzzy attack: Fuzzy attacks in dataset are injected every 0.5 milliseconds with CAN messages where the CAN ID and DATA values are forged randomly.
- 3) Spoofing attack: Spoofing attacks in dataset are messages injected every 1 millisecond with a specific CAN ID, e.g., related to RPM/Gear.

Table II indicates the number of normal and injected messages in each attack dataset. In order to summarize the spatial-temporal details of normal CAN bus traffic during the operation of a real vehicle, we first investigated the communication patterns of different CAN IDs. Since the dataset is not publicly available as to the receiving sender and receiver of the data, the paper analyzes the CAN protocol table of a brand from our laboratory. We find that an ECU has a fixed set of CAN IDs (e.g. EMS, containing 0x101, 0x278, 0x281) and that the recipients of the different CAN IDs are also fixed (e.g. 0x101, containing TCU, ESP, EPB, T-BOX). This is the original purpose to design a single-frame detection model capable of tracing unauthorized ECUs and protecting unattacked ECUs.

Additionally, the frequency of the different IDs is fixed by the vehicle manufacturer. It is worth noting that important automotive components have a higher priority. Hence, time-series features are reflected in the ID of the CAN data. Despite the fact that there are also event-triggered messages with

TABLE IV: ANALYZE THE MESSAGE FRAME OF THE SELECTED ID

ID	Transmitter	1	2	3	4	5	6	7	8
0x260	N/A	05	22	00	30	FF	99	63	38
									0B
									1A
									29
0x316	RPM	05	22	6A	0B	21	18	00	7F
				16		22			
				23	3A	23			
				24	1A	24			
0x43F	GEAR	10	50	60	FF	46	28	0A	00
								0C	
								10	
								F0	

variable frequency, the set of commands is also fixed. The details are shown in Table III.

Table IV displays some CAN message of different CAN IDs from the dataset. we observe that they have certain fixed byte constants (e.g., the first 7 bytes of ID '0x260'), as well as fields that change more frequently (e.g., the third bytes of ID '0x316'), but only in a certain range. there are distinct spatial characteristics of the data field, useful for modeling the normal behavior of the CAN packet, and also inspire the requirement to design attention convolution blocks.

To more visually observe the byte change patterns, the data fields for each message are displayed in a heat map, as shown in Fig.5. In order to apparently visualize the differences in variation of the each byte, this paper presents 100 consecutive communication messages based on three important CAN IDs such as gear and speed. There is a certain period of color shade variation at ID = 0x260 and ID = 0x43F, while the messages sent by the RPM-specific IDs are clearly irregular, corresponding to the summary in Table IV.

In conclusion, spatial-temporal details are useful for modeling the normal behavior of CAN packets, and attention also focuses on bytes that change frequently and time-series important relationships, thus helping the model to quickly detect violations and determine the targeted traffic.

IV. INTRUSION DETECTION SYSTEM USING SPATIAL-TEMPORAL CORRELATION FEATURE

A. dataset Preprocessing

The neural network-based approach to training in the original CAN dataset is impractical. Hence, dataset pre-processing is a necessary part of the training prior to training. The payload field, as shown in Table IV, is 8 bytes, of which each byte is represented by two numbers in hexadecimal format. In fact, the public source dataset was progressively judged and found to contain a large number of data frames that were inferior to 8 bytes or irregular. To ensure uniformity of model input, we filled in the missing data frames with "00" in two scenarios: 1) where the data frame is less than 8 bytes; 2) where only the single digit "0" is used to represent a byte. Afterward, we split and transformed the arbitration bits and data domain in the dataset into a trainable dataset containing 19 features,

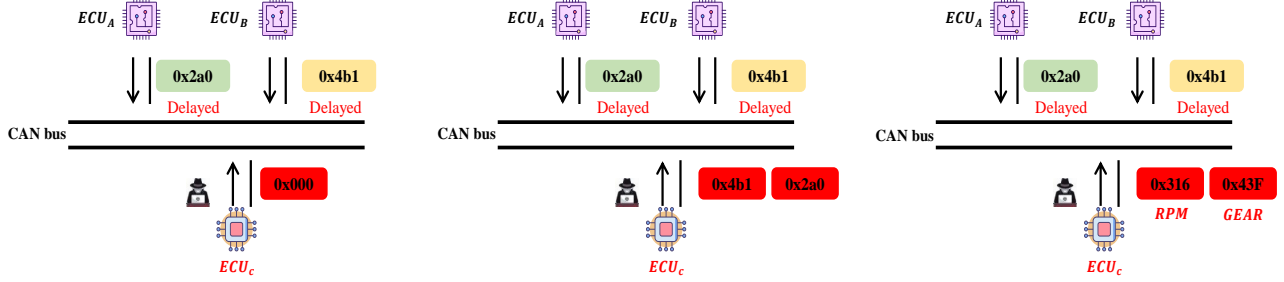


Fig. 4: Illustration of the injection process of utilized in-vehicle intrusion dataset.

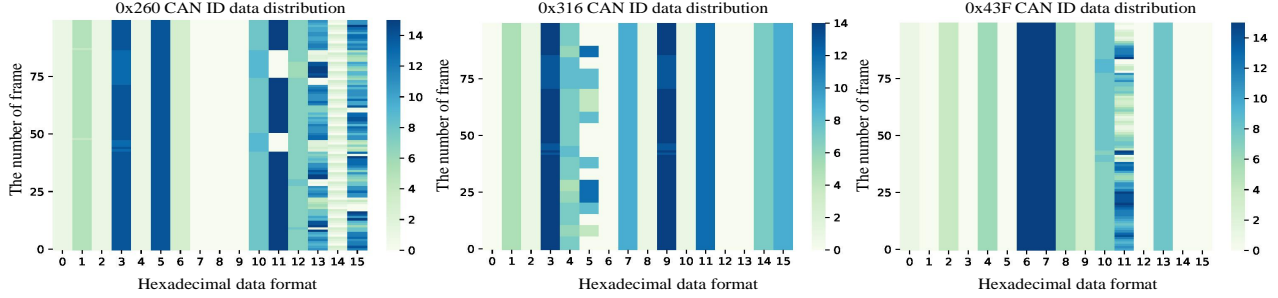


Fig. 5: Value distribution by Heatmap in hexadecimal form of each bit of CAN frame for different ID includes ID = 0x260, ID = 0x316, and ID=0x43F.

respectively 16 features in 8 bytes of the data domain. In particular, the CAN ID is partitioned into 3 bits in order to harmonize the operation with the data field being split. On the one hand, the combination of the hexadecimal features of the original multi-bit will not be too far removed from the data field features due to the introduction of time-frequency features; on the other hand, all messages provided by the public dataset have only 3 valid bits in hexadecimal.

In addition, the values of all features will be converted to decimal values from hexadecimal values. After implementing missing data padding and decimal conversion to meet the basic inputs to the model, several additional data pre-processing steps still need to be completed. First, the network traffic data frame type is encoded using a label encoder, which is used to convert categorical features into numerical features to support the input of ML&DL algorithms, as many ML&DL algorithms cannot directly support string features [24]. Afterward, the network dataset is normalized by the Min-Max algorithm, as the features collected in network traffic data often have a wide range of differences that impose model deviations and emphasize only large-scale features. Furthermore, the ML&DL model is proven to perform more convergent easily on normalized dataset [37]. Hence, the data normalized by the Min-Max method is calculated:

$$X_{\text{norm}} = \frac{X - X_{\text{min}}}{X_{\text{max}} - X_{\text{min}}} \quad (1)$$

The method implements equal scaling of the original data, where X_{norm} is the normalized data, X is the original data, and X_{max} and X_{min} are the maximum and minimum values of the original dataset respectively. Table V presents the CAN data that is available as input to the model, where the

TABLE V: THE PRE-PROCESSED DATASET IS REPRESENTED WITH THE LABELS DIVIDED INTO NORMAL (0) AND INTRUSION (1)

ID			DATA								Label
ID1	ID2	ID3	Byte1	Byte2	Byte3	Byte4	Byte5	Byte6	Byte7	Byte8	
0.2	0.06	0.4	0	0.13	0.4	0	0.13	0.13	0	0.4	0
0.06	0.53	1	1	0.33	0	0	0	0.2	0	0	0
0	0	0	0.93	0.73	0	0	0	0.8	0	0	0
			0	0	0	0	0	0	0	0	1
			0	0	0	0	0	0	0	0	0

former three columns are the CAN ID feature fields, the next eight columns in each message present 16 data domain fields, and the last column represents the label in digital form for each message. In addition, the first two rows represent the distribution for normal CAN data features, while the distribution for injection attacks is the third row. For multi-frame detection, encoder requires an additional image conversion step that splits the collected data set into 64×19 2-D images. After the normalization is complete, in order to prevent the same attacks from appearing in both the test and the segmented attack data, dataset division is for 10-fold cross-validation via StratifiedKFold function in sklearn library.

B. STC-IDS Model Design

The STC-IDS consists of two steps: encoding and detection. The encoder is an analysis of the spatial-temporal characteristics of the CAN data, based on attention, capturing the important relationships in it; the detector achieves anomaly classification to the input features.

1) *STC-IDS for Single-Frame Detection*: From the perspective of single-frame data detection, our aim is to retrieve the illegally controlled source ECU in conjunction with the CAN ID (i.e., accurate identification of every abnormal traffic). In training phase, we extract spatial features at one-dimensional data by CNN. Considering that the input to the network is only 1×19 , in order not to invalidate the extracted features, the spatial extraction component is consisted by three convolution blocks and a global pooling. The convolution block consists of a 1-D convolution layer, a batch-normalization layer, and an activation function ReLU. The batch-normalization allows the model to discard the learning of biases, and global pooling are used to reduce the number of parameters. In particular, the batch-normalization makes the convolution output of the model homogeneous. The ReLU function make the network own nonlinear properties. The global pooling serves to assist the model in searching for where critical bytes are and reducing redundant information.

Simultaneously, an improved LSTM structure with attention, called A-LSTM, receives the input single CAN frame as a multivariate time series with a single time step. Attention actually mimics a visual mechanism of the human brain, seen as an automatic weighting scheme [38]. For the single-frame model, after the dimensional shuffling layer processing that used to increase the speed of multivariate processing, features are fed into the A-LSTM blocks. To prevent over-fitting, the discard layer plays a crucial role. The A-LSTM component is to discover crucial byte changes by the following formula.

$$a_b = \exp(u_b^T * u_w) / \sum_b \exp(u_b^T * u_w) \quad (2)$$

Where u_w is the weight matrix, and u_b means the implicit representation of the hidden state h_b at computation feature bit b . The u_b is calculated as follows.

$$u_b = \tanh(W_w h_b + b_w) \quad (3)$$

Where W_w is the weight matrix and b_w is the bias. Afterward, we attain the attention probability distribution value at each byte. Finally, we will compute the final feature vector v as follows.

$$v = \sum_b a_b * h_b \quad (4)$$

In Fig.6, we present a parallel feature extraction classification model for single-frame detection. Both features are finally aggregated by the fully connected layers. We refer to it as the CAN valuable feature for spatial-temporal correlation under multi-view learning. Finally, it is fed into the final classification component, which specific elaboration in algorithm 1.

2) *STC-IDS for Multi-Frame Detection*: To further elevate the efficiency, multi-frame detection IDS is constructed. In other words, during data pre-processing, the model retrieves a continuous CAN message matrix, aggregated from 64 consecutive CAN messages, where 64 represents the length of the historical time series that the model could recall. For supervised learning, data frames that contain one or more injection messages are marked as attack CAN images, while

Algorithm 1 STC-IDS for single-frame

```

1: Require: Input Data  $X$ , LSTM-Times = 2, Convolution-
   Times = 3;
2: Temporal Phase:
3:  $X_{\text{temporal}} = \text{Dimension shuffle}(X)$ ;
4: for Times to LSTM-Times do
5:    $h_b = \text{LSTM}(X_{\text{temporal}})$ ;
6:    $u_b = \tanh(W_w h_b + b_w)$ ;
7:    $a_b = \exp(u_b^T * u_w) / \sum_b \exp(u_b^T * u_w)$ ;
8:    $v = \sum_t a_b * h_b$ ;
9:    $X_{\text{temporal}} = \text{Dropout}(v)$ ;
10: end for
11: Spatial Phase:
12:  $X_{\text{spatial}} = X$ ;
13: for Times to Convolution-Times do
14:    $X = \text{Conv1D}(X_{\text{spatial}})$ 
15:    $X = \text{Batch-Normalization}(X)$ 
16:    $X = \text{ReLU}(X)$ 
17:    $X_{\text{spatial}} = X$ 
18: end for
19:  $X_{\text{spatial}} = \text{Global-Pooling}(X_{\text{spatial}})$ 
20:  $X_{\text{spatial-temporal}} = \text{Concatenate}(X_{\text{spatial}}, X_{\text{temporal}})$ 
21:  $X_{\text{spatial-temporal}} = \text{Dense}(X_{\text{spatial-temporal}})$ 
22:  $\hat{y} = \text{Softmax}(X_{\text{spatial-temporal}})$ 

```

data frames that do not contain injection messages are marked as normal CAN images.

As shown in Fig.7, the constructed CAN image dataset are fed under both parallel networks. The temporal feature extraction module remains the same structure, but the input is a time series in two dimensions so that A-LSTM pays more attention to important relationships from previous time series. After the dimensional shuffling layer swap out the time dimension of the time series, the processed time series are fed into the A-LSTM blocks. However, the three main parameters in the single-frame temporal attention model, i.e. u_b, h_b, a_b , need to be redefined as u_t, h_t, a_t . u_t indicates the implicit representation of the hidden state h_t at computation time t , while a_t represents the final computed attention value.

Moreover, the spatial feature extraction component is inspired by the VGGNet. It keeps feature extraction capability, but the channel number and convolution layers are modified in the architecture to adapt CAN dataset. It is composed of three convolution blocks, but one convolution module consists of a 2-D convolution layer, a batch normalization layer, and a max-pooling layer.

Owing to the convolution layer having the feature of shared weight, the complexity of the model decreases, and the efficiency of the reasoning increases as a result. For instance, if we process a $64 \times 19 \times 3$ feature map into a $62 \times 17 \times 6$ volume, the full-connected layer requires $(64 \times 19 \times 3) \times (62 \times 17 \times 6) = 22M$ weights, while the convolution layer via 3×3 convolution kernels only require $(3 \times 3 \times 3) \times 6 = 162$ weights. Fig.8 illustrates the difference between convolution and fully connected layer computations. The multi-frame detection also has the capability to remove redundant information, and reduce the

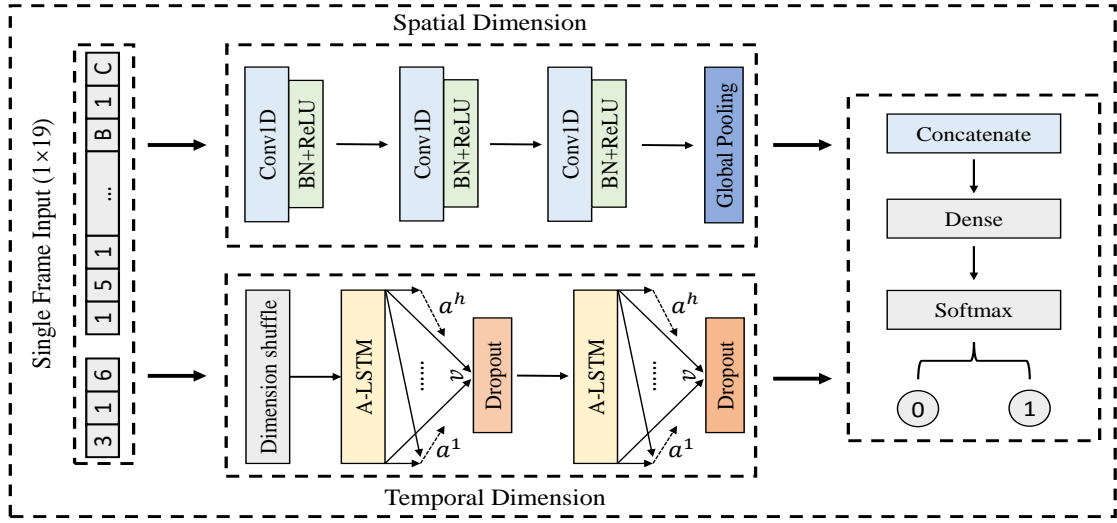


Fig. 6: To illustrate the single-frame detection neural network.

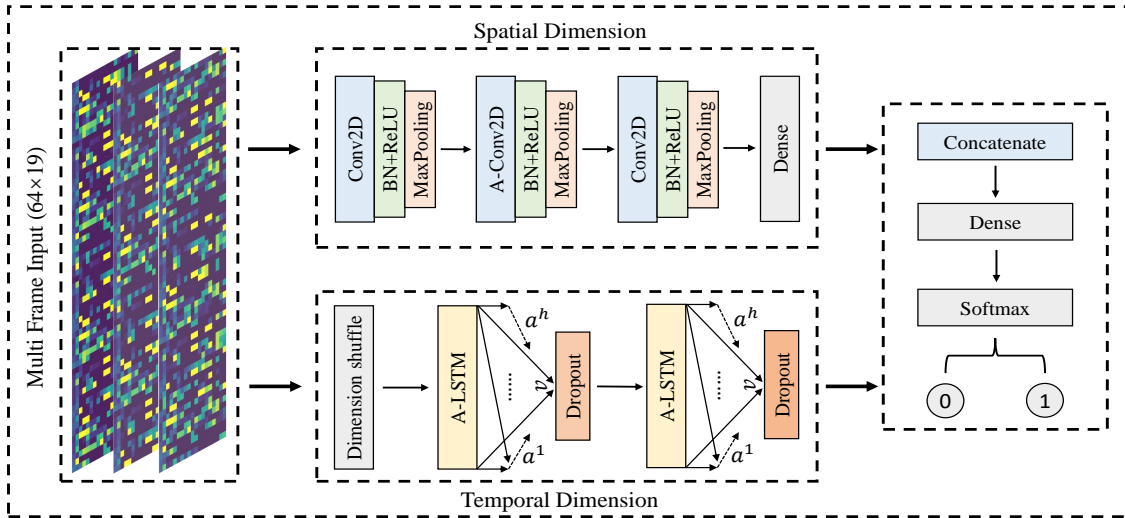


Fig. 7: To illustrate the multi-frame detection neural network.

computational effort with the help of the max-pooling layer. The convolution block maps the raw data to the hidden feature space, thereby, in order to improve the performance of the CNN network, it performs the task of feature engineering. The fully connected layer serves to map the learned "distributed feature representation" to the sample markup space. Hence, spatial-temporal correlation features are extracted in a parallel network and are finally aggregated by a fully connected layer as a classification.

Most importantly, we have modified the second convolution component somewhat, which is a convolution component with visual attention, called A-Conv2D. The core idea of it is to help the network extract and represent the information most relevant to the target. For instance, when viewing a photograph, we usually focus on the individuals in the picture so that we are able to summarize the critical information in the picture. Observing Table II and the heat map in Fig.5, there are clearly key information changes in the bytes as a

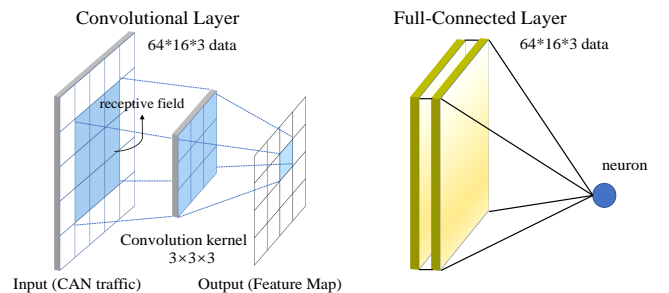


Fig. 8: In the computation of neurons in the convolution and fully connected layers, it is clear that the former is smaller than the latter, due to the dense connectivity.

CAN image. Recently, channel attention and spatial attention are mentioned in the CNN [39], Inspired by the idea, the proposed structure is in such ways that the convolution network

finds where the key information is and where the channel features are learned, giving the model the capability to self-select important features and eliminate the feature engineering step. Hence, the intermediate layer network of convolution branches will be obtained a convolution feature with spatial attention and channel attention. This additional structure is essentially cascaded over the original network with the purpose of better extracting more valuable features. All in all, attention convolution module features are calculated as follows.

$$\begin{aligned} F_{\text{merge}} &= M_s(F_c) \otimes F_c \\ &= M_s(M_c(F) \otimes F) \otimes (M_c(F) \otimes F) \end{aligned} \quad (5)$$

where F_{merge} is the aggregated feature. M_c , M_s are channel attention weight coefficients and spatial attention weight coefficients, respectively, while F is the input feature and F_c is the channel attention feature.

In Fig.9, the feature maps built by the first convolution block are extracted by the attention convolution component to fuse features. Firstly, the max-pooling and avg-pooling layers aggregate spatial attention information to generate two different spatial context descriptions; immediately afterward the multi-layer perceptron (MLP) adds the two features together and through a Sigmoid activation function to obtain the weight coefficients M_c . Finally, the weight coefficients M_c are multiplied by the original features F to obtain the channel attention features F_c . Note that the MLP neural network is weight-sharing.

$$\begin{aligned} M_c &= \sigma(\text{MLP}(\text{AvgPool}(F)) + \text{MLP}(\text{MaxPool}(F))) \\ &= \sigma(W_1(W_0(F_{\text{avg}}^c)) + W_1(W_0(F_{\text{max}}^c))) \end{aligned} \quad (6)$$

$$F_c = M_c \otimes F \quad (7)$$

where σ is the activation function, W_0 and W_1 are the weight matrices of the convergence layer.

The spatial attention module has been proven to be a stable complement to channel attention information because of its ability to mine where the key features are. Similar to channel attention, given an $H \times W \times C$ feature F_c , two $H \times W \times 1$ channel descriptions are obtained by averaging pooling and max pooling in one channel dimension, respectively, and stitching the two descriptions together by channel. Then, a 2×2 convolution layer with Sigmoid activation function is applied to obtain the weight coefficients M_s . Finally, the spatial-channel attention aggregation feature F_{merge} is obtained by multiplying the weight coefficients M_s with the feature F_c .

$$\begin{aligned} M_s &= \sigma(f^{2 \times 2}([\text{AvgPool}(F_c); \text{MaxPool}(F_c)])) \\ &= \sigma(f^{2 \times 2}([\text{F}_{\text{avg}}^s; \text{F}_{\text{max}}^s])) \end{aligned} \quad (8)$$

With the fusion of the two network structures, the network layers thus become deeper, making it easy to over-fit the network. For better generalization of the model, $L2$ regularization is set in the network layer to limit the gradient.

Finally, two detection model are calculated the predict \hat{y}_i via the follow formula, where f_x is the combining features. \hat{y}_i present the probability distribution over target classes zero

Algorithm 2 STC-IDS for multi-frame

```

1: Require: Input Data  $X$ , LSTM-Times = 2, Convolution-
   Times = 3;
2: Temporal Phase:
3:  $X_{\text{temporal}} = \text{Dimension shuffle}(X)$ ;
4: for Times to LSTM-Times do
5:    $h_t = \text{LSTM}(X_{\text{temporal}})$ ;
6:    $u_t = \tanh(W_w h_t + b_w)$ ;
7:    $a_t = \exp(u_t^T * u_w) / \sum_t \exp(u_t^T * u_w)$ ;
8:    $v = \sum_t a_t * h_t$ ;
9:    $X_{\text{temporal}} = \text{Dropout}(v)$ ;
10: end for
11: Spatial Phase:
12:  $X_{\text{spatial}} = X$ ;
13: for Times to Convolution-Times do
14:    $F = \text{Conv2D}(X_{\text{spatial}})$ 
15:    $F = \text{Batch-Normalization}(X)$ 
16:    $F = \text{ReLU}(F)$ 
17:    $F = \text{Max-Pooling}(F)$ 
18:   if Times == 2 then
19:      $M_c = \text{Channel Attention}(F)$ 
20:      $F_c = M_c \otimes F$ 
21:      $M_s = \text{Spatial Attention}(F_c)$ 
22:      $F_{\text{merge}} = M_s \otimes F_c$ 
23:      $X_{\text{spatial}} = F_{\text{merge}}$ 
24:   else
25:      $X_{\text{spatial}} = F$ 
26:   end if
27: end for
28:  $X_{\text{spatial}} = \text{Dense}(X_{\text{spatial}})$ 
29:  $X_{\text{spatial-temporal}} = \text{Concatenate}(X_{\text{spatial}}, X_{\text{temporal}})$ 
30:  $X_{\text{spatial-temporal}} = \text{Dense}(X_{\text{spatial-temporal}})$ 
31:  $\hat{y} = \text{Softmax}(X_{\text{spatial-temporal}})$ 

```

and one. Specifically, the multi-frame model is described in algorithm 2

$$\begin{aligned} \hat{y}_i &= p(c = i | x) \\ &= \text{softmax}(w \cdot f_x + b) \quad (\text{for } i = 0, 1) \end{aligned} \quad (9)$$

To maximize the probability p , we need to continuously optimize by back propagation to reduce loss, fitting the network to the best structure, loss function is calculated as follows.

$$\begin{aligned} L &= \frac{1}{N} \sum_i L_i + \lambda \|w\|^2 \\ &= \frac{1}{N} \sum_i -[y_i \cdot \log(p_i) + (1 - y_i) \cdot \log(1 - p_i)] + \lambda \|w\|^2 \end{aligned} \quad (10)$$

V. EVALUATION

We now validate that the spatial-temporal correlation feature can be used to detect anomaly frames, and evaluate the performance on a CAN bus prototype and real vehicles.

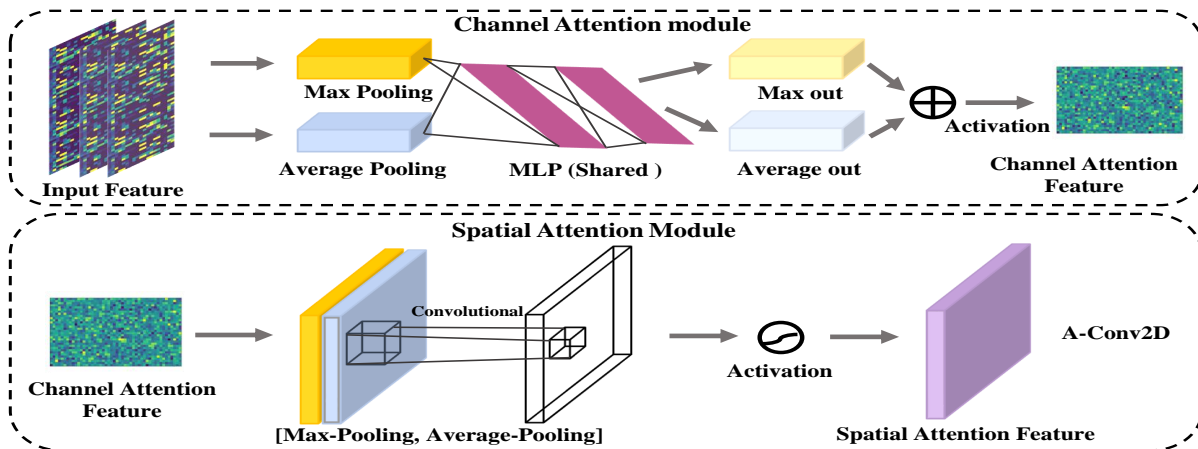


Fig. 9: Schematic representation of the CAN image computed in the attention convolution module. The channel module utilizes the shared network to output the max-pooling and avg-pooling computed features; the spatial attention module pools the pooling output along the channel axis and computes the final features through the convolution layer.

A. Evaluation Metrics and Experiment Environment

In this paper, statistical metrics TP (true positive) and TN (true negative) are introduced to indicate the number of frames correctly classified as attack and normal, while metrics FP (false positive) and FN (false negative) are introduced to indicate the number of data frames that are misclassified as attack and normal. The model accuracy formula is as follows.

$$Acc = (TP + TN)/(TP + FN + FP + TN) \quad (11)$$

Precision (P) and recall (R) are considered as evaluation metrics to assess classification performance. Precision refers to the rate at which the actual data frame labels are detected correctly, while recall represents the proportion of all attack frame samples that end up in the attack frame class and is calculated as follows.

$$P = TP/(TP + FP) \quad (12)$$

and

$$R = TP/(TP + FN) \quad (13)$$

The experimental evaluation also calculates an F1 score, which is based on a harmonic average of the percentages of detection and detection completeness. F1 scores are often used to measure classification performance when the data are unevenly distributed and are calculated as follows.

$$F1 = 2 \times P \times R/(P + R) \quad (14)$$

Additionally, the false negative rate (FNR) and the error rate (ER) are one way of assessing classification performance; FNR is the proportion of frames that are not detected as belonging to the attack frame and ER is the proportion of frames that are incorrectly classified, calculated as follows.

$$FNR = FN/(TP + FN) \quad (15)$$

and

$$ER = FN + FP/(TN + TP + FN + FP) \quad (16)$$

The two models designed in this paper were trained offline based on the dataset, while the testing phase was based on real vehicles, injected with malicious frames of the same rules, to check the performance and efficiency of the models. The following is the experimental training and testing environment.

- 1) Intel(R) Core (TM) i7-9500U CPU@3.6GHz
- 2) RAM:64.0 GB
- 3) GPU RTX 2080 Ti (Training environment)
- 4) CAN Test, NVIDIA Jetson AGX Xavier (16GB) (Testing environment)

B. Hyperparameter Selection and Optimization

The selection of hyperparameters is crucial in network performance and inference efficiency. Currently, automated Hyperparametric Optimization (HPO) services and toolkits address the constant trial-and-error steps of deep learning developers [40]. In this paper, Bayesian Optimization (BO) automatic parametric tuning is used in order to quickly determine hyperparameters. It is a typical method applied to global optimization problems. Compared to grid search and stochastic search, BO is more computationally efficient and requires fewer attempts to find the optimal set of hyperparameters [37].

Based on the BO optimization library provided by Keras-tuner and on a 10-fold cross-validation dataset, we selected important hyperparameters such as learning rate (1e-2, 1e-3, 1e-4, 1e-5, 1e-6), optimizer (e.g., Adam, SGD, RMSprop), dropout rate, and filters. Afterward, we set the optimization goal to validate the accuracy (Val-Acc), a maximum number of trials of 10, and train the model 3 times per trial. Finally, the optimization results will present the set of top 3 hyperparameters for performance.

As shown in Table VI, the average accuracy on the cross-validation set reach 99.98% in the single-frame model when setting the learning rate 1e-6, the dropout rate 0.4, the filters 16, 32, 128, the dense layer 64, and the optimizer Adam, while the accuracy is achieved up to 99.96% to the multi-frame model under the optimal hyperparameters.

TABLE VI: EFFECT OF HYPERPARAMETERS ON MODEL PERFORMANCE UNDER AUTOMATED HPO

Model type	Learning rate	Dropout rate	Filters	Dense	Optimizer	Val-Acc
Single Frame	1e-6	0.4	16,32,128	64	Adam	0.9998
	1e-6	0.4	8,96,32	48	Adam	0.9935
	1e-6	0.4	8,16,192	80	Adam	0.9869
Multi Frame	1e-2	0.4	64,16,32	128	Adam	0.9996
	1e-2	0	8,16,32	128	Adam	0.9993
	1e-2	0	24,80,96	256	Adam	0.9992

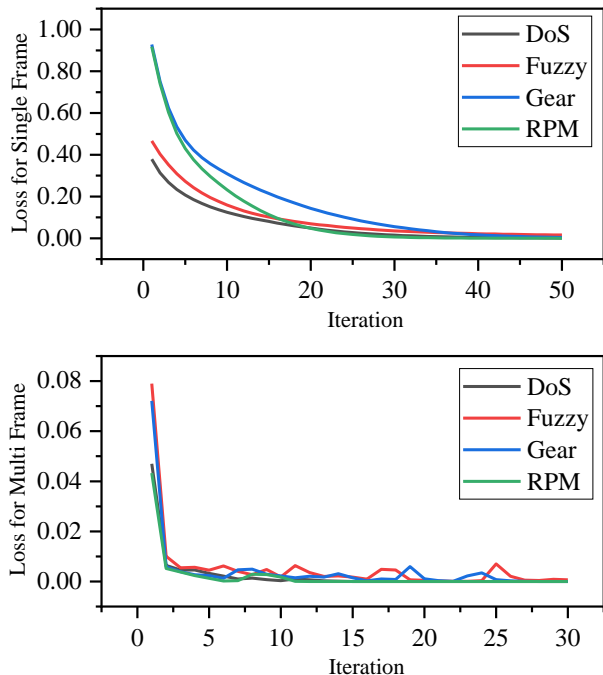


Fig. 10: To illustrate training loss on each dataset in single-frame (a) and multi-frame (b) algorithms.

Interestingly, the inference speed of the model was significantly accelerated aided by the optimal hyperparameters. Despite the higher detection performance was obtained by the single-frame model, the inference speed is slower. Relative to multi-frame, it took 50 iterations to converge, whereas multi-frame model only took 30 generations. Fig. 10 shows the iterative training losses for each dataset. It can be observed that since the DoS attack disrupts the frequency of injection, both models learn the patterns and converge quickly. However, as the complexity of the attack data increases, the fuzzy and malfunction attacks injected with random data converge slower in the single-frame model, while the training loss convergence fluctuates significantly in the multi-frame model.

C. Detection Metrics Evaluation and Comparison

After training the best two models according to the set hyperparameters, Fig. 11 shows the detection performance of the models in terms of ER and FNR for the four-attack testing sets in 30 repeated experiments. The two proposed models, both in terms of FNR, and ER, presents stable performance to detect DoS attacks with mean values of 0.0047%, 0.0204%, 0.0159% and 0.0094%, respectively. On the contrary, the fuzzy

TABLE VII: IDS PERFORMANCE COMPARISON WITH BASELINE METHODS

DoS	ER (%)	FNR (%)	P (%)	R (%)	F1 (%)
STC-IDS for Single Frame	0.02	0.01	99.95	99.99	99.96
STC-IDS for Multi Frame	0.01	0.02	99.91	99.97	99.94
3-LSTM [26]	0.07	0.22	1.0	99.78	99.88
DCNN [11]	0.03	0.10	1.0	99.89	99.95
DAE [41]	-	0.12	91.27	99.88	95.36
OTIDS [42]	-	26.2	99.90	73.80	84.88
Fuzzy	ER (%)	FNR (%)	P (%)	R (%)	F1 (%)
STC-IDS for Single Frame	0.05	0.04	99.97	99.95	99.96
STC-IDS for Multi Frame	0.09	0.07	99.90	99.92	99.91
3-LSTM [26]	0.84	0.65	99.36	99.16	99.26
DCNN [11]	0.18	0.35	99.95	99.65	99.80
DAE [41]	-	3.74	90.05	96.26	93.05
OTIDS [42]	-	29.79	99.14	70.21	82.20
Gear	ER (%)	FNR (%)	P (%)	R (%)	F1 (%)
STC-IDS for Single Frame	0.04	0.03	99.97	99.96	99.97
STC-IDS for Multi Frame	0.07	0.03	99.94	99.96	99.95
3-LSTM [11]	0.24	0.32	99.75	99.68	99.72
DCNN [26]	0.05	0.11	99.99	99.89	99.94
DAE [41]	-	18.2	94.63	81.80	87.75
OTIDS [42]	-	28.35	99.83	71.65	83.42
RPM	ER (%)	FNR (%)	P (%)	R (%)	F1 (%)
STC-IDS for Single Frame	0.04	0.03	99.98	99.96	99.97
STC-IDS for Multi Frame	0.07	0.03	99.95	99.96	99.96
3-LSTM [11]	0.13	0.30	1	99.71	99.85
DCNN [26]	0.03	0.05	99.99	99.94	99.96
DAE [41]	-	4.27	95.73	95.73	92.10
OTIDS [42]	-	28.32	99.81	71.68	83.43

attacks shows greater fluctuations in detection performance owing to the random injection of packet, but the mean values of FNR are still 0.0328% and 0.0413%, as well as ER get 0.0435% and 0.0864%.

Also, for Gear and RPM attacks, although FNR and ER are higher than for Dos attacks, they achieves stable and better results compared to Fuzzy attacks. The single-frame detector averages 0.0251% and 0.0353% for the Gear attack on both metrics, while the multi-frame detector obtains 0.0294% and 0.0704%. Similarly, when detecting RPM attacks, the performance of both models is similar to Gear attacks.

Notably, the single-frame detection model requires mining the characteristics of different CAN packets, thus exhibiting fluctuations in FNR and ER values that are greater than the multi-frame model. Taking into account the detection efficiency, the multi-frame model, although fast and stable, has a higher false alarm rate than the former.

To reflect the advantages of our scheme, Table VII lists the detection performance of STC-IDS when compared with previous work, where the highest performance values are highlighted in bold, and "-" only means that the scheme has not been tested on this metric. The results indicate clearly that the performance of the scheme is improved on all dataset, and the false positive rate is significantly reduced. It can be seen that the model captures the spatial-temporal details of network traffic remarkably well and enhances the spatial-temporal feature correlation better.

Evidently, we observe that the STC-IDS single-frame model achieves a stable precision (99.97%), a higher recall (99.96%),

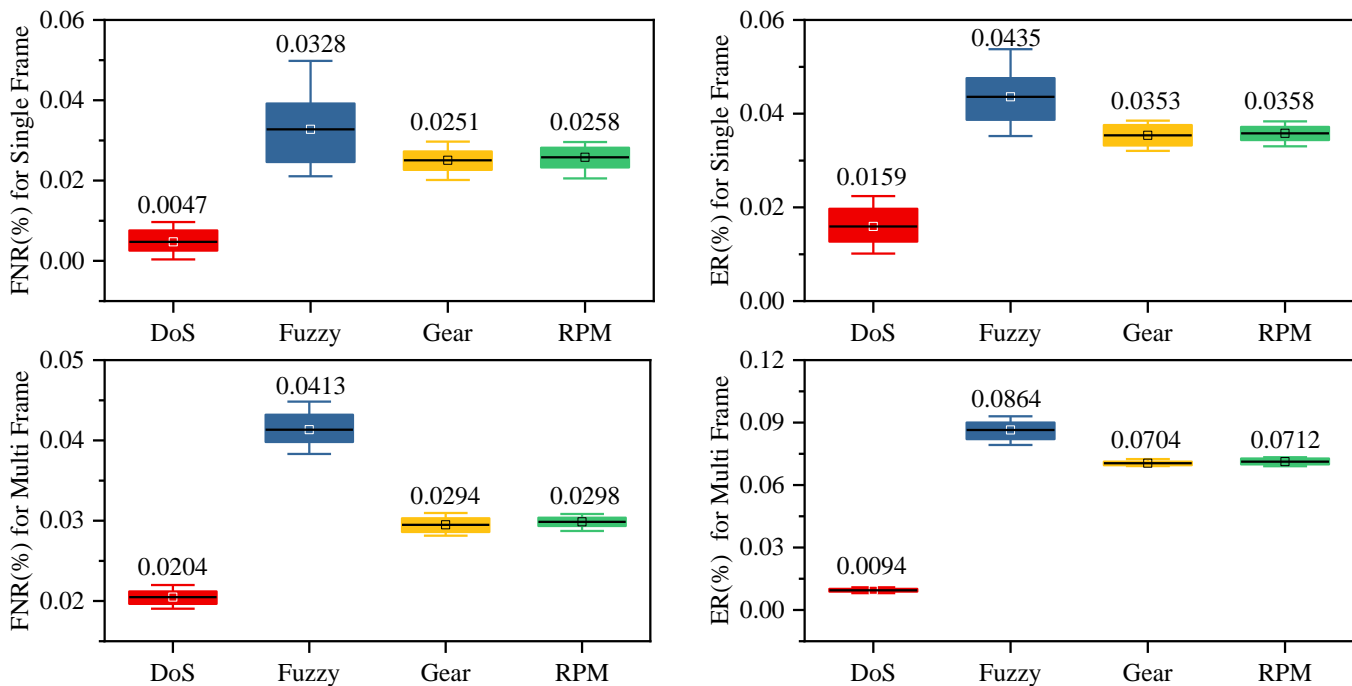


Fig. 11: Box-plots of single-frame and multi-frame models measuring FNR and ER in 30 replicate experiments.

and an outstanding F1-score (99.96%) in average as compared to a threshold (OTIDS), classification (DCNN), prediction (3-LSTM), and clustering (DAE) based models. In contrast, for the STC-IDS multi-frame model, performance solely decreases by an average of 0.04% precision, 0.01% recall and 0.03% in F1-score while maintaining efficiency.

The 3-LSTM scheme shows high accuracy and unstable recall because of the unconsidered spatial correlation, resulting in a low F1 score and a large gap between FNR and ER with our scheme and DCNN. DCNN is currently one of the best models for in-vehicle intrusion detection, but the stacking of convolutions is ineffective in capturing the temporal relationships of the inputs. As a result, the single-frame model reduces the FNR and ER by 90% and 33% over the DCNN scheme for DoS attacks, while the multi-frame model reduces the FNR by 80% and the ER by 66%. More notably, for complex fuzzy attacks, only 0.04% FNR and 0.05% ER are achieved on the single-frame model. In addition, the FNR is slightly improved on the Gear and RPM dataset. Meanwhile, the ER gets approximate performance compared with the DCNN model.

Compared to the other two methods, the DAE model, with its lack of labeling constraints, encompasses a bigger reduction in performance than the primary 3 schemes, achieving better performance (95.36% in F1-score) only on DoS attacks. Similarly, the OTIDS exhibited a high accuracy rate and extremely low recall, resulting in an FNR of over 25%, reflecting a relatively low F1 score. Thus, the robust spatial-temporal correlation feature demonstrates its blessings in terms of improved detection performance and lower false-positive rates.



Fig. 12: To illustrate the testing experiment environment.

D. Time Cost in Real Vehicle

This work first implemented single frame detection in terms of security considerations. Although the performance is improved over previous algorithms, the efficiency is not guaranteed. However, time and resources are the major limitations to applying deep learning models to real-world vehicle IDS. Therefore, STC-IDS based on multi-frames also was proposed by us. Obviously, Significant improvements were made in terms of model convergence time as shown in subsection 5.2. To test the efficiency for our model a resource-constrained in-vehicle network, the model was tested on an in-vehicle class device the NVIDIA Jetson AGX Xavier. Note that only 4GB of video memory was allocated for testing. The CAN Test software injected the attack traffic by connecting to the OBD-II port, as shown in Fig.12.

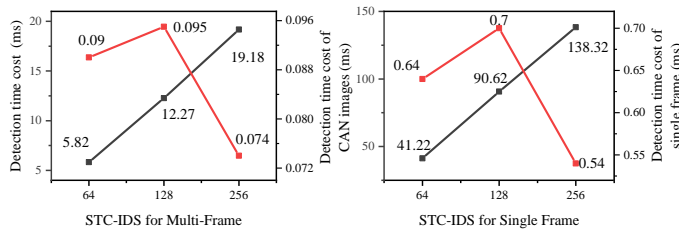


Fig. 13: Testing time of our models on different batches and average efficiency.

In Fig.13, we give the time (in milliseconds) cost to detect CAN frame anomalies for batches of 64, 128, and 256 of two model, where the red line represents the average time cost per frame. For the single-frame detection model, Calculating the average detection time per frame we found to increase and then decrease, being 0.64 ms, 0.70 ms, and 0.54 ms. This truly shows that the model is constantly learning as it reasoned, thus making it easier to catch malicious features later on. However, at the fastest detection time of 0.54ms, it can be estimated that the model can detect 1851 messages in 1s, while CAN frames transmit approximately 2000 messages in 1s, showing that the efficiency is limited.

In contrast, the multi-frame model detected the CAN images in three batches, achieving 0.09 ms, 0.09 ms, and 0.074 ms time cost on average. It is worth mentioning that the model practically detects 64 frames of messages continuously. This means that the model can inference about five times the number of CAN transmission messages in 1s. Hence, the proposed model has the feasibility for real-time detection.

E. Discussion and Limitations

The study presented two enhanced spatial-temporal features analyzing IDS for detecting single CAN messages and consecutive CAN frame based on publicly injection attack dataset. Experiments showed that the proposed STC-IDS single-frame model exhibited good detection performance. Similarly, the STC-IDS multi-frame model improved efficiency while ensuring performance.

Although the detection efficiency of the single-frame model is very limited, we believe that the model will be suitable for real-time detection when using higher-performance computing devices, as it is necessary to track unauthorized ECUs in conjunction with CAN ID indexing. It is worth noting that the time-cost detection of proposed methods is based on in-vehicle edge computing and autonomous driving platform from our research group. Although it has satisfied the requirement for intrusion detection in real-time, when in a real environment, all tasks are simultaneously are performed, there may be some impact and more research is needed in terms of implementation.

Moreover, the division of CAN ID in the scheme is limited to public dataset. In order to accommodate more realistic in-vehicle messages, the division should be completed in practice by considering both standard frames (11 bits) and extended frames (29 bits). However, it is straightforward only to modify the dimensionality of the input for the proposed model. Most

importantly, the model has a fundamental limitation in terms of detecting unlearned types of attacks as it is based on supervised learning. To address this challenge, more research is needed on unknown attack detection using models with generative functions such as adversarial training, auto-encoder.

VI. CONCLUSIONS

This work focuses on building an automotive intrusion detection model to learn the temporal and spatial characteristics of in-vehicle network traffic in order to build enhanced spatial-temporal correlation features. Our proposed STC-IDS model is implemented based on the encode-detection architecture. The coding layer is constructed as a parallel network in both temporal and spatial terms base on LSTM and CNN. The introduction of A-LSTM and A-Conv2D helps the model uncover important relationships between keyword node variation and temporal order. Spatial-temporal correlation features are fed into the detection layer to complete anomaly detection.

Both models achieve optimal hyperparameter selection with Bayesian optimization, reducing the number of iterations and elevating accuracy. Compared to previous schemes, our system achieves a better performance by testing the four publicly attack dataset, i.e., DoS, Fuzzy, Gear, and RPM, especially in the FNR and ER metrics.

Although this study achieves security protection of the CAN bus, there is still much room for improvement, especially unknown attack detection. In future work, we will consider how to express realistic unknown attack messages, improving model robustness and generalization capabilities. Data annotation is also a tedious task, but unsupervised algorithms are one of the solutions and still need continuous research to improve performance.

REFERENCES

- [1] H. M. Song and H. K. Kim, "Self-supervised anomaly detection for in-vehicle network using noised pseudo normal data," *IEEE Transactions on Vehicular Technology*, vol. 70, no. 2, pp. 1098–1108, 2021.
- [2] S.-H. Kim, S.-H. Seo, J.-H. Kim, T.-M. Moon, C.-W. Son, S.-H. Hwang, and J. W. Jeon, "A gateway system for an automotive system: Lin, can, and flexray," in *2008 6th IEEE International Conference on Industrial Informatics*. IEEE, 2008, pp. 967–972.
- [3] C. Miller and C. Valasek, "Remote exploitation of an unaltered passenger vehicle," *Black Hat USA*, vol. 2015, no. S 91, 2015.
- [4] S. Checkoway, D. McCoy, B. Kantor, D. Anderson, H. Shacham, S. Savage, K. Koscher, A. Czeskis, F. Roesner, T. Kohno *et al.*, "Comprehensive experimental analyses of automotive attack surfaces," in *USENIX Security Symposium*, vol. 4, no. 447-462. San Francisco, 2011, p. 2021.
- [5] J. Petit and S. E. Shladover, "Potential cyberattacks on automated vehicles," *IEEE Transactions on Intelligent transportation systems*, vol. 16, no. 2, pp. 546–556, 2014.
- [6] E. Aliwa, O. Rana, C. Perera, and P. Burnap, "Cyberattacks and countermeasures for in-vehicle networks," *ACM Computing Surveys (CSUR)*, vol. 54, no. 1, pp. 1–37, 2021.
- [7] T. Hoppe, S. Kiltz, and J. Dittmann, "Security threats to automotive can networks—practical examples and selected short-term countermeasures," in *International Conference on Computer Safety, Reliability, and Security*. Springer, 2008, pp. 235–248.
- [8] I. Rouf, R. D. Miller, H. A. Mustafa, T. Taylor, S. Oh, W. Xu, M. Gruteser, W. Trappe, and I. Seskar, "Security and privacy vulnerabilities of in-car wireless networks: A tire pressure monitoring system case study," in *USENIX Security Symposium*, vol. 10, 2010.
- [9] W. Wu, R. Li, G. Xie, J. An, Y. Bai, J. Zhou, and K. Li, "A survey of intrusion detection for in-vehicle networks," *IEEE Transactions on Intelligent Transportation Systems*, vol. 21, no. 3, pp. 919–933, 2019.

- [10] D. He, S. Chan, Y. Zhang, C. Wu, and B. Wang, "How effective are the prevailing attack-defense models for cybersecurity anyway?" *IEEE Intelligent Systems*, vol. 29, no. 5, pp. 14–21, 2013.
- [11] H. M. Song, J. Woo, and H. K. Kim, "In-vehicle network intrusion detection using deep convolutional neural network," *Vehicular Communications*, vol. 21, p. 100198, 2020.
- [12] H. Qin, M. Yan, and H. Ji, "Application of controller area network (can) bus anomaly detection based on time series prediction," *Vehicular Communications*, vol. 27, p. 100291, 2021.
- [13] H. Olufowobi, C. Young, J. Zambreno, and G. Bloom, "Saiducant: Specification-based automotive intrusion detection using controller area network (can) timing," *IEEE Transactions on Vehicular Technology*, vol. 69, no. 2, pp. 1484–1494, 2019.
- [14] S. Tariq, S. Lee, Y. Shin, M. S. Lee, O. Jung, D. Chung, and S. S. Woo, "Detecting anomalies in space using multivariate convolutional lstm with mixtures of probabilistic pca," in *Proceedings of the 25th ACM SIGKDD International Conference on Knowledge Discovery & Data Mining*, 2019, pp. 2123–2133.
- [15] C. Zhang, D. Song, Y. Chen, X. Feng, C. Lumezanu, W. Cheng, J. Ni, B. Zong, H. Chen, and N. V. Chawla, "A deep neural network for unsupervised anomaly detection and diagnosis in multivariate time series data," in *Proceedings of the AAAI Conference on Artificial Intelligence*, vol. 33, no. 01, 2019, pp. 1409–1416.
- [16] H. Sun, M. Chen, J. Weng, Z. Liu, and G. Geng, "Anomaly detection for in-vehicle network using cnn-lstm with attention mechanism," *IEEE Transactions on Vehicular Technology*, vol. 70, no. 10, pp. 10880–10893, 2021.
- [17] I. Studnia, E. Alata, V. Nicomette, M. Kaâniche, and Y. Laarouchi, "A language-based intrusion detection approach for automotive embedded networks," *International Journal of Embedded Systems*, vol. 10, no. 1, pp. 1–12, 2018.
- [18] T. Dagan and A. Wool, "Parrot, a software-only anti-spoofing defense system for the can bus," *ESCAR EUROPE*, p. 34, 2016.
- [19] K.-T. Cho and K. G. Shin, "Fingerprinting electronic control units for vehicle intrusion detection," in *25th {USENIX} Security Symposium ({USENIX} Security 16)*, 2016, pp. 911–927.
- [20] W. Choi, K. Joo, H. J. Jo, M. C. Park, and D. H. Lee, "Voltageids: Low-level communication characteristics for automotive intrusion detection system," *IEEE Transactions on Information Forensics and Security*, vol. 13, no. 8, pp. 2114–2129, 2018.
- [21] H. M. Song, H. R. Kim, and H. K. Kim, "Intrusion detection system based on the analysis of time intervals of can messages for in-vehicle network," in *2016 international conference on information networking (ICOIN)*. IEEE, 2016, pp. 63–68.
- [22] C. Young, J. Zambreno, H. Olufowobi, and G. Bloom, "Survey of automotive controller area network intrusion detection systems," *IEEE Design & Test*, vol. 36, no. 6, pp. 48–55, 2019.
- [23] M.-J. Kang and J.-W. Kang, "Intrusion detection system using deep neural network for in-vehicle network security," *PloS one*, vol. 11, no. 6, p. e0155781, 2016.
- [24] L. Yang, A. Moubayed, and A. Shami, "Mth-ids: A multitiered hybrid intrusion detection system for internet of vehicles," *IEEE Internet of Things Journal*, vol. 9, no. 1, pp. 616–632, 2021.
- [25] S. Tariq, S. Lee, and S. S. Woo, "Cantransfer: transfer learning based intrusion detection on a controller area network using convolutional lstm network," in *Proceedings of the 35th Annual ACM Symposium on Applied Computing*, 2020, pp. 1048–1055.
- [26] K. Pawelec, R. A. Bridges, and F. L. Combs, "Towards a can ids based on a neural network data field predictor," in *Proceedings of the ACM Workshop on Automotive Cybersecurity*, 2019, pp. 31–34.
- [27] A. Tomlinson, J. Bryans, and S. A. Shaikh, "Towards viable intrusion detection methods for the automotive controller area network," in *2nd ACM Computer Science in Cars Symposium*, 2018, pp. 1–9.
- [28] W. Wang, M. Zhu, X. Zeng, X. Ye, and Y. Sheng, "Malware traffic classification using convolutional neural network for representation learning," in *2017 International Conference on Information Networking (ICOIN)*. IEEE, 2017, pp. 712–717.
- [29] L. Yang, A. Moubayed, I. Hamieh, and A. Shami, "Tree-based intelligent intrusion detection system in internet of vehicles," in *2019 IEEE global communications conference (GLOBECOM)*. IEEE, 2019, pp. 1–6.
- [30] A. U. Jadhav and N. Wagdarikar, "A review: Control area network (can) based intelligent vehicle system for driver assistance using advanced rise machines (arm)," in *2015 International Conference on Pervasive Computing (ICPC)*. IEEE, 2015, pp. 1–3.
- [31] O. Y. Al-Jarrah, C. Maple, M. Dianati, D. Oxtoby, and A. Mouzakitis, "Intrusion detection systems for intra-vehicle networks: A review," *IEEE Access*, vol. 7, pp. 21266–21289, 2019.
- [32] R. I. Davis, A. Burns, R. J. Bril, and J. J. Lukkien, "Controller area network (can) schedulability analysis: Refuted, revisited and revised," *Real-Time Systems*, vol. 35, no. 3, pp. 239–272, 2007.
- [33] K. Tindell, A. Burns, and A. J. Wellings, "Calculating controller area network (can) message response times," *Control engineering practice*, vol. 3, no. 8, pp. 1163–1169, 1995.
- [34] S. Punnekkat, H. Hansson, and C. Norstrom, "Response time analysis under errors for can," in *Proceedings Sixth IEEE Real-Time Technology and Applications Symposium. RTAS 2000*. IEEE, 2000, pp. 258–265.
- [35] V. S. Barletta, D. Caivano, A. Nannavecchia, and M. Scalera, "Intrusion detection for in-vehicle communication networks: An unsupervised kohonen som approach," *Future Internet*, vol. 12, no. 7, p. 119, 2020.
- [36] E. Seo, H. M. Song, and H. K. Kim, "Gids: Gan based intrusion detection system for in-vehicle network," in *2018 16th Annual Conference on Privacy, Security and Trust (PST)*. IEEE, 2018, pp. 1–6.
- [37] L. Yang and A. Shami, "On hyperparameter optimization of machine learning algorithms: Theory and practice," *Neurocomputing*, vol. 415, pp. 295–316, 2020.
- [38] D. Bahdanau, K. Cho, and Y. Bengio, "Neural machine translation by jointly learning to align and translate," *arXiv preprint arXiv:1409.0473*, 2014.
- [39] S. Woo, J. Park, J.-Y. Lee, and I. S. Kweon, "Cbam: Convolutional block attention module," in *Proceedings of the European conference on computer vision (ECCV)*, 2018, pp. 3–19.
- [40] T. Yu and H. Zhu, "Hyper-parameter optimization: A review of algorithms and applications," *arXiv preprint arXiv:2003.05689*, 2020.
- [41] T. Amarbayasgalan, B. Jargalsaikhan, and K. H. Ryu, "Unsupervised novelty detection using deep autoencoders with density based clustering," *Applied Sciences*, vol. 8, no. 9, p. 1468, 2018.
- [42] H. Lee, S. H. Jeong, and H. K. Kim, "Otidis: A novel intrusion detection system for in-vehicle network by using remote frame," in *2017 15th Annual Conference on Privacy, Security and Trust (PST)*. IEEE, 2017, pp. 57–5709.



Mu Han (Member, IEEE) received the Ph.D. degree in Computer Science from Nanjing University of Science and Technology. She is an Associate Professor with the School of Computer Science and Communication Engineering, Jiangsu University. Her primary research interests are in the areas of Cryptography, Security and Communication in-vehicle networks, the design of security protocols for smart cars and Information Security.



Pengzhou Cheng is currently pursuing the M.S. Degree with the Department of Computer Science and Communication Engineering, Jiangsu University. His primary research interests include privacy information protection, Machine Learning, security of Electronic Control Units in vehicular networks, controller area network security, intrusion detection system.



Fengwei Zhang received the Ph.D. degree in Computer Science from George Mason University. He is an Associate Professor with Department of Computer Science and Engineering, Southern University of Science and Technology. He was an Assistant Professor and the Director of the COMPASS Lab with Department of Computer Science, Wayne State University. His primary research interests are in the areas of systems security, with a focus on trustworthy execution, hardware-supported security, transparent malware analysis, and plausible deniability encryption.